Article

Performance of wedge-shaped block armoring for embankment dams and levees in a singular testing facility at quasi-prototype size

F.J. Caballero [1, 2, *], M.Á. Toledo [1], R. Morán [1, 3], and J. Peraita [1,2]

[1] Universidad Politécnica de Madrid (UPM). SERPA dam safety research group. E.T.S. de Ingenieros de Caminos, Canales y Puertos. Calle Profesor Aranguren, s/n. 28040 Madrid, Spain. ORCID of the authors, respectively: 0000-0001-5102-5943; 0000-0002-7594-7624; 0000-0002-0031-1605 and 0000-0003-0583-7144. miguelangel.toledo@upm.es (M.Á.T.); r.moran@upm.es (R.M.); j.peraita@upm.es(J.P.)

[2] ACIS innovation+engineering S.L. (ACIS2in). Calle Planeta Urano 13, P18 2ºA, 28983 Parla (Madrid).

[3] International Center for Numerical Methods in Engineering (CIMNE). Universidad Politécnica de Cataluña, Campus Norte UPC, 08034 Barcelona, Spain.

* Correspondence: franciscojavier.caballero@upm.es (F.J.C.); Tel.: +34-616-978-633

Abstract: The article presents the results and conclusions of a series of tests of wedge-shaped blocks armoring carried out on a new experimental facility (*'Hydraulic Experimentation Facility - Luis Ruano'*) in quasi-prototype conditions. The article describes the singular testing facility that was built at the inlet channel of the Acequia de Sora channel, immediately upstream of the Laverné reservoir (Zaragoza, Spain). The inflow of the testing facility has a maximum discharge of 9 m^3s^{-1}. The aim is to perform experimental research on technologies to protect embankment dams and dikes against overflowing erosion under quasi-prototype conditions. The results of the tests showed the ability of the WSBs to withstand high unit discharges under extremely negative conditions. Furthermore, conclusions were drawn about potential threats to the sound behavior of the armor.

Keywords: Wedge-shaped block, WSB, overtopping, overflowing erosion, dam protection, dam spillway, dam safety, embankment dam, precast concrete, ACUÑA

1. Introduction and background.

In recent years, there has been an increase in regulatory requirements in many fields of society, including critical infrastructures, such as dams.

Regarding the hydrological safety of dams, these safety criteria are manifested, for example, in the increase in the return periods required for design floods, or in the updating of hydrological studies with longer data series and reliable data proposed in the safety reports of the existing dams. In some cases, longer return period floods can lead to overtopping of the dam (due to depletion of the freeboards) if no adaptation measures are carried out in their spillways or outlet works. Overtopping is a process for which most dams are not designed. For this reason, the risk of serious damage to them, or even dam failure, increases under these circumstances, especially in earth dams, where it is the main cause of dam failure [1].

The need to adapt to the new regulatory framework, together with the economic situation of recent years, has forced the approach of other nonconventional solutions, with lower costs compared to conventional solutions traditionally used. This paradigm shift, imposed by current market conditions, has led the Federal Emergency Management

Preprints (www.preprints.org) | NOT PEER-REVIEWED | Posted: 25 November 2022 doi:10.20944/preprints202211.0478.v1

Agency (FEMA) of the United States of America to publish a technical guide on dam protections against overtopping [2]. This guide establishes general design criteria but does not include sizing methodologies or recommendations on the calculation of this type of infrastructure, as is the case for wedge-shaped block (WSB) protections.

To improve this situation, a series of R&D projects have been developed in Spain since 2011, which, based on the knowledge developed by the Moscow Institute of Civil Engineering in the late 1960s [3], and from the advances carried out by the same organization [4,5], the Construction Industry Research and Information Association (CIRIA) [3,6-10], Colorado State University and Bureau of Reclamation (USA) [11-16], and the Instituto Superior Técnico of Lisbon [17-21], among others [22], have led to the obtaining a new prototype of wedge-shaped precast concrete block, the ACUÑA block [23] (patent ES 2595852 B2), as well as the definition of a methodology for the protection design with this block implemented in a software (DIABLO) that allows its calculation and optimization [24].

The last of these projects has involved the construction of a large-scale experimental facility to carry out tests on a quasi-prototype scale located immediately upstream of the Laverné reservoir at Ejea de los Caballeros (Zaragoza, Spain), having been named '*Hydraulic Experimentation Facility - Luis Ruano*' (HEFLR) in memory of one of the research promoters. The facility has been used to carry out an experimental validation on a prototype scale of the ACUÑA.

It is important to highlight the importance of this type of prototype testing to validate the operation of the block that is intended to be used by dam (or levee) owners, given that, in most cases, they require references for use in operating conditions with high flow rates. units to accept its use in real cases.

It should be noted that the HEFLR is designed to be a singular research infrastructure to test new technologies for the protection of dams and levees against overtopping on a prototype scale.

2. Materials and Methods

2.1. Experimental Facility

The new experimental facility has been developed in the auxiliary inlet channel of the Acequia de Sora channel (**Figure 1**), immediately upstream of the Laverné reservoir in Ejea de los Caballeros (Zaragoza, Spain). From the Acequia de Sora channel, a maximum discharge of 7 m^3s^{-1} (eventually, up to 9 m^3s^{-1} can be supplied to this facility).

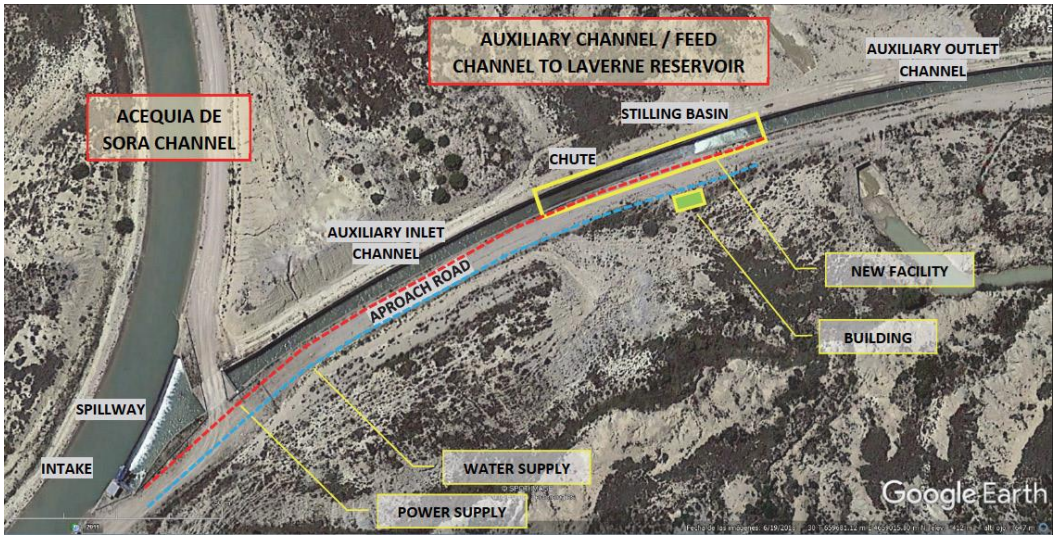

Figure 1. Location of test facilities

The auxiliary channel has an intake work at the upstream edge and a length that exceeds 600 m to the reservoir, at the downstream end. The flow into the auxiliary channel

Preprints (www.preprints.org) | NOT PEER-REVIEWED | Posted: 25 November 2022 doi:10.20944/preprints202211.0478.v1

is supplied from the intake, located on the right bank of the Acequia de Sora channel. The inlet consists of a motorized rectangular flow control gate of 2.50 x 3.00 m (**Figure 2**a) with an invert elevation of 419.89 m above the sea level (m.a.s.l.) and a 30 meters long side-spillway, curved in plan, located immediately downstream of the gate (**Figure 2**b). The elevation of the crest is 422.83 m.a.s.l. (Video 1 and Video 2 in Supplementary Materials).

Figure 2. Intake work in the Acequia de Sora channel: (a) View from downstream of the flow control gate in operation. (b) Flow control structure on the left and side spillway from the Acequia de Sora to the auxiliary channel.

The experimental facility was built inside the existing auxiliary channel, approximately 90 m downstream of the intake work. The chute section has the following characteristics: 52.25 m long reinforced concrete channel with a rectangular cross section of 4.00 m wide, with variable height from 3.66 to 3.75 m in the first 41.80 m, and 3.75 to 5.27 m in the last 10.45 m. The longitudinal slope of the chute is 14.57% in the first 41.80 m and 22.88% in the last 10.45 m. The invert elevation of the upstream section of the chute is 419.67 m.a.s.l. At the end of the chute there is a 14.63 m long stilling basin with a 4.00 m wide and 5.25 m high rectangular section with a horizontal slab at an elevation of 411.62 m.a.s.l. The basin ends at a 1.03 m high step, which is the upstream end of the last stretch of the auxiliary channel (at elevation 412.65 m.a.s.l.).

The HEFLR located inside the chute consists of an upstream pressure channel, an intermediate supply tower, made of steel, and the test chute (**Figure 3a** and **Figure 3b**).

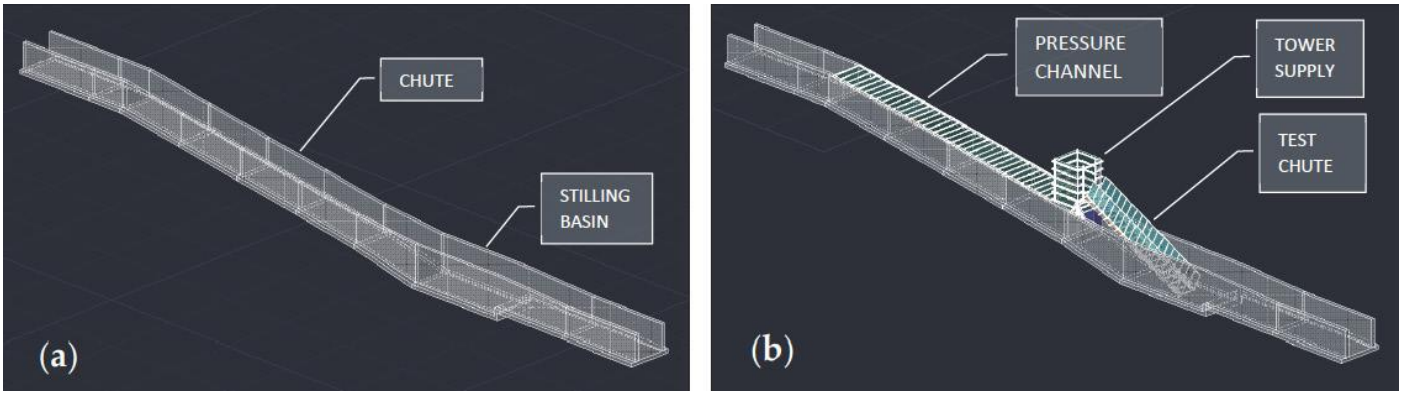

Figure 3. 3D view of the auxiliary channel (a) Initial situation (b) Situation after the installation of HEFLR

The pressure channel was designed to have the highest water elevation in the tower supply. (Figure 3b), with negligible head loss for the test flows and sectional capacity. The pressure channel is 38 meters long and consists of a simple lining of the existing channel using reinforced concrete alveolar slabs (except at the end of the pressure channel close to the tower supply, in which the last two slabs are replaced by metallic plates) (**Figure 4**a, b and c). The alveolar concrete slabs are attached to the top of the side walls of the concrete

 doi:10.20944/preprints202211.0478.v1

chute and are supported by a rigid skeleton made up of metal beams anchored in the reinforced concrete of the existing walls (**Figure 4**d). A sealing treatment has been provided in the slab-slab and slab-pocket joints (**Figure 4**e).

The material of the supply tower is steel. The horizontal section of the tower is square, with a side of 4.00 m. The maximum height is 9.23 m above its support on the channel supply slab and 5.71 m above the current walls of the auxiliary channel (**Figure 5**a). At the top of its downstream side, the tower has a 1.82 m wide and 3.49 m high opening that fits into the upstream end of the testing chute (**Figure 5**b). This opening is reinforced by a series of metal profiles that ensure its structural strength and functionality. The elevation of the lower edge of the opening is 419.70, coinciding with the elevation of the base of the test chute. In the lower part of the tower, on the downstream side, there is a wall gate of 3.93 x 2.87 m (**Figure 5**c) that must be closed to use the facility. A 250-mm diameter butterfly valve (**Figure 5**c) was installed on the gate for emptying the storage water and reducing pressure on the wall gate to facilitate its opening.

Preprints (www.preprints.org) | NOT PEER-REVIEWED | Posted: 25 November 2022 doi:10.20944/preprints202211.0478.v1

Figure 4. (**a**) View of HEFLR from the right bank of the auxiliary channel. (**b**) View of the interior of the auxiliary channel from upstream of the pressure channel. (**c**) Storage of the alveolar slabs used to cover the pressure channel. (**d**) Metallic frames used to support the alveolar slabs of the pressure channel and the metallic plates on the connection to the tower supply. (**e**) Detail of the sealing between the alveolar slabs and between the slabs and the channel walls (view from inside the pressure channel).

Preprints (www.preprints.org) | NOT PEER-REVIEWED | Posted: 25 November 2022 doi:10.20944/preprints202211.0478.v1

Figure 5. (a) General view of the supply tower (b) Photographic montage of the water inside the supply tower (left) exiting towards the test chute (right). (c) Wall gate of the supply tower and 250-mm diameter butterfly valve to facilitate its manoeuvre by emptying the water retained upstream.

The test chute is a modular steel structure supported on a metallic platform (**Figure 6**a) with a total width of 3.00 m and a maximum vertical drop of 7.05 m. The chute is equipped with a 0.50-m-wide platform for inspection during tests beside the right wall (**Figure 6**b). The width of the chute can be adapted from minimum of 0.5 meter to maximum of 2 meter with intervals of half a meter. The configuration selected for the tests had an intermediate longitudinal wall of width of 2 m with a 0.40 m high made of steel. The longitudinal slope can be changed from 1H:1V to 3.5H:1V with increments of 0.5H:1V (**Figure 7**). Such a change can be achieved thanks to the support of the testing chute at its upstream end with a horizontal axis of rotation that prevents its displacement but allows the rotation. The change in longitudinal slope requires the addition or removal of chute

Preprints (www.preprints.org) | NOT PEER-REVIEWED | Posted: 25 November 2022 doi:10.20944/preprints202211.0478.v1

modules (**Figure 7a and 7b**) to adapt the corresponding length. The configuration selected for the tests was 2H:1V. The side walls of the chute are 2.50 m high measured in the perpendicular direction to the bottom. The right-side wall has clear methacrylate windows to allow observation during the tests (**Figure 6**).

Figure 6. (a) General view from the right bank of the test chute before being lowered to the bottom of the auxiliary channel **(b)** Photo of the inspection windows from the side platform of the chute. In the background, the supply tower.

When the testing chute is not used, it remains elevated from the auxiliary channel, supported by a metal beam at its downstream end (**Figure 8b**). The chute can be lowered (or lifted) from its lower end using a crane (Video 3 in Supplementary Materials)

This crane helps to operate the wall gate of the supply tower too (**Figure 8a and b**).

Preprints (www.preprints.org) | NOT PEER-REVIEWED | Posted: 25 November 2022 doi:10.20944/preprints202211.0478.v1

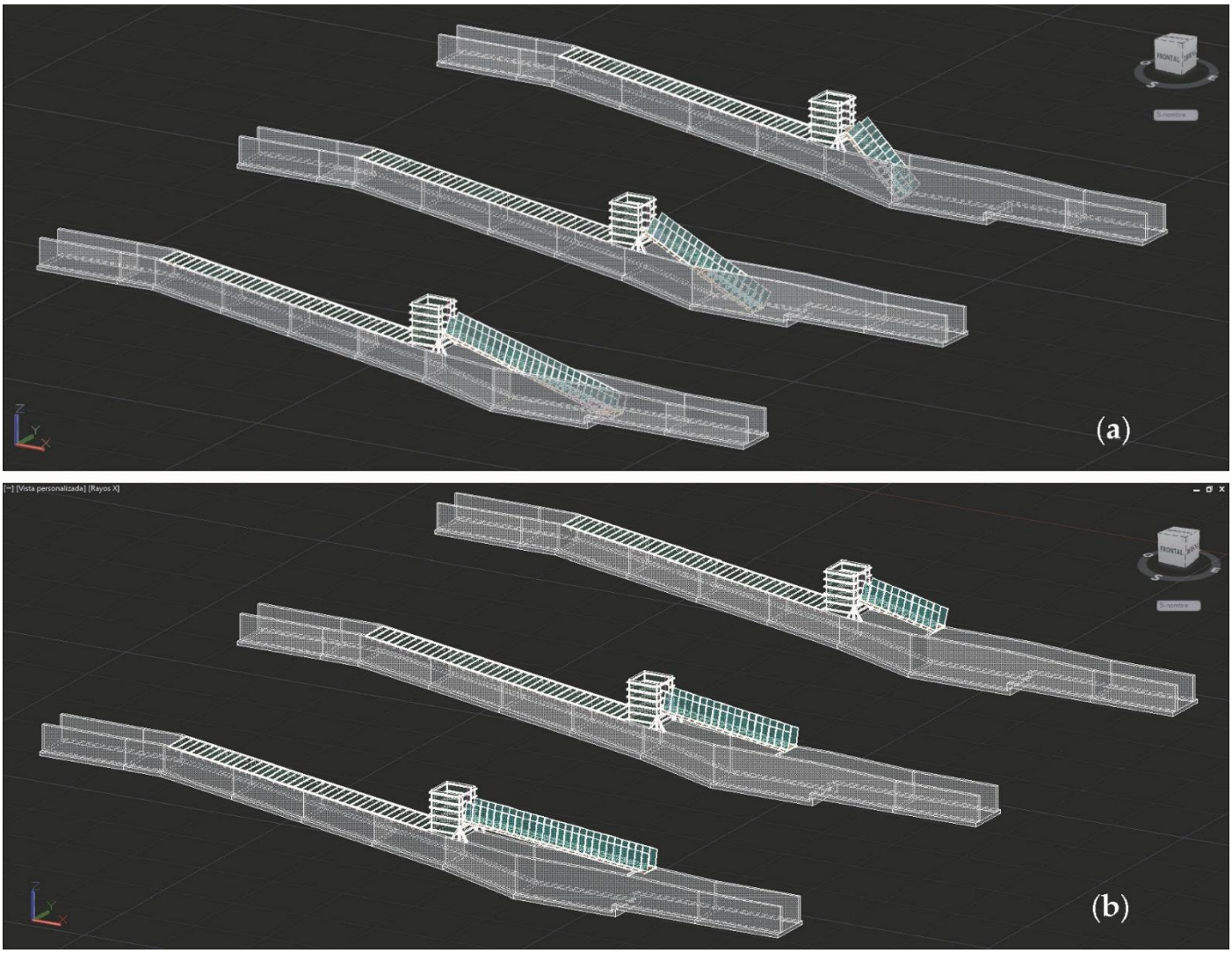

Figure 7. Schemes of the testing chute with different slopes in the test chute in lowered position, ready for testing (a) and lifted (b).

Figure 8. (**a**) Picture of the crane lifting the test chute. (**b**) Picture of the testing chute once lifted.

2.2. Description of the WSB armoring

Preprints (www.preprints.org) | NOT PEER-REVIEWED | Posted: 25 November 2022 doi:10.20944/preprints202211.0478.v1

The different WSB models tested in each trial were placed on a 0.20 m thick bedding layer formed by homogeneous gravel of particle size in the range of 12 to 20 mm. This granular layer was extended over a wire mesh with 40-mm openings fixed at the bottom of the testing chute (**Figure 9**).

Figure 9. Picture of the placement of the WSB on the gravel bedding layer.

The WSB model used in the tests was ACUÑA® (**Figure 10**) with three 3 different sizes (**Table 1**):

- Small block, weighing 5.0 kg, 167.0 mm wide (A) and 243.3 mm long (L).
- Medium block, weighing 15.0 kg, 250.0 mm wide and 364.3 mm long.
- Large block, weighing 35.0 kg, 330.0 mm wide and 401.8 mm long.

Note that the dimensions are proportional for every size of the block. Thus, the scale between the small and large WSB is 0.51, and 0.76 between the medium and large.

Preprints (www.preprints.org) | NOT PEER-REVIEWED | Posted: 25 November 2022 doi:10.20944/preprints202211.0478.v1

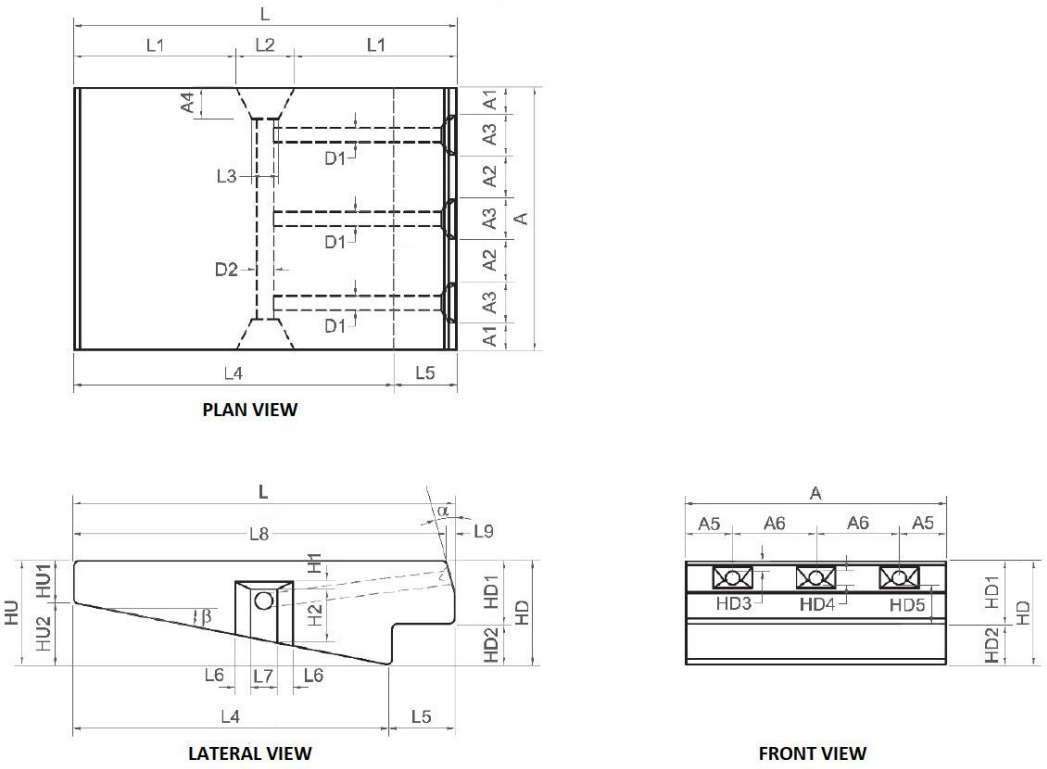

Figure 10. Geometrical parameters of the ACUÑA® blocks.

Table 1. Dimensions and weights of the three sizes of the tested blocks.

BLOCK	L	L1	L2	L3	L4	L5	L6	L7	L8	L9	a
SIZE	mm	mm	mm	mm	mm	mm	mm	mm	mm	mm	º
Small	243.3	103.0	37.0	103.3	17.0	203.3	40.0	10.0	238.6	4.8	15.0
Medium	364.3	154.2	55.4	154.7	25.4	304.4	59.9	15.0	357.1	7.1	15.0
Large	480.8	203.5	73.1	204.2	33.6	401.8	79.0	19.8	471.4	9.4	15.0

BLOCK	A	A1	A2	A3	A4	A5	A6	HU	HU1	HU2	b
SIZE	mm	mm	mm	mm	mm	mm	mm	mm	mm	mm	º
Small	167.0	17.5	28.5	25.0	19.5	30.0	53.5	65.9	27.2	38.7	10.8
Medium	250.0	26.2	42.7	37.4	29.2	44.9	80.1	98.7	40.7	57.9	10.8
Large	330.0	34.6	56.3	49.4	38.5	59.3	105.7	130.3	53.7	76.5	10.8

BLOCK	Weight	HD	HD1	HD2	HD3	HD4	HD5	H1	H2	D1	D2
SIZE	kg	mm	mm	mm	mm	mm	mm	mm	mm	mm	mm
Small	5.0	65.9	40.0	25.9	6.3	8.7	25.0	5.0	34.2	9.0	11.0
Medium	15.0	98.7	59.9	38.8	9.4	13.0	37.4	7.5	51.3	13.5	16.5
Large	35.0	130.3	79.0	51.3	12.4	17.2	49.4	9.9	67.7	17.8	21.7

The WSBs were placed in horizontal rows, beginning from the bottom row and working upward. The WSB placement was done with a staggered configuration of the longitudinal joints among the blocks. To do so, half-pieces of WSB were placed at the end of alternative horizontal rows, as shown in **Figure 11**.

Preprints (www.preprints.org) | NOT PEER-REVIEWED | Posted: 25 November 2022 doi:10.20944/preprints202211.0478.v1

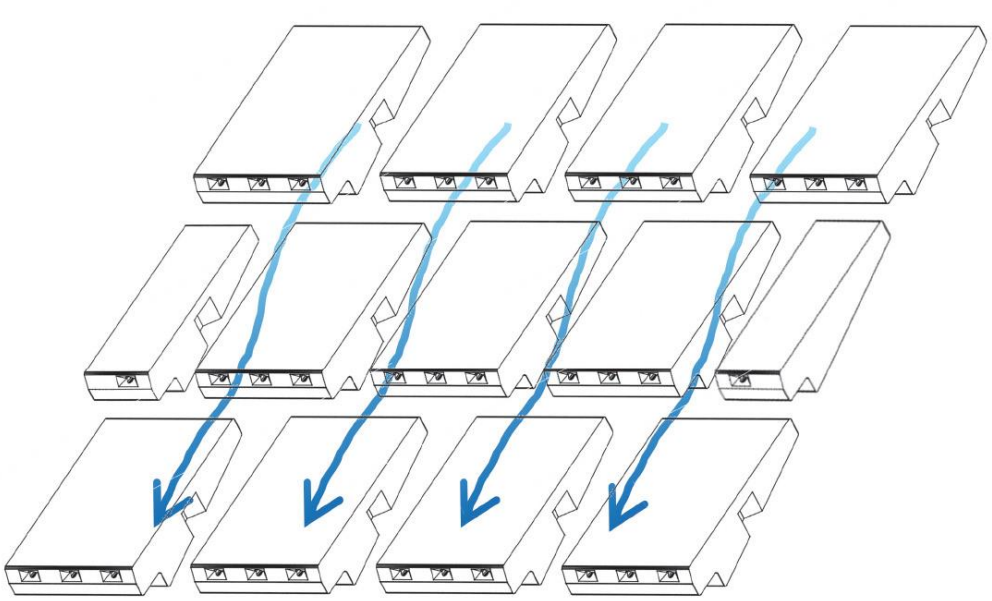

Figure 11. Scheme of the placement of WSB in rows and the creation of staggered longitudinal joints by using half-WSB.

Two types of WSB were tested in each of the two sessions of tests. To do this, the flume was divided into two halves, 1 m wide each, symmetrical along the longitudinal axis of the chute. The division was made by a longitudinal intermediate wall formed by a 400 mm high metallic sheet, welded to the bottom of the chute (**Figure 12**).

Figure 12. Picture of the intermediate wall dividing the two areas with different WSB sizes.

In the first test session, small and medium sizes of WSB were used. The small WSB were placed along the right half of the test channel in 80 rows, plus 1 end with trimmed blocks for the upstream row. In total, 440 WSB, 80 half-blocks, plus 6 blocks for the upstream row (row# 81). Medium WSBs were placed in 53 rows, plus an additional row at the upstream end with trimmed blocks. In total, 186 WSB, 52 half-blocks, and 3 blocks, plus 2 half-blocks, for the upstream row (row# 54). Additionally, an eyebolt was installed on some WSB for block extraction tests (**Figure 13**). The pieces to be extracted were in the central block of six selected rows and distributed along the channel in rows #16, #26, #36, #44, #54 and #64 for the small blocks, and #10, #18, #24, #30, #36 and #42 for medium blocks.

Preprints (www.preprints.org) | NOT PEER-REVIEWED | Posted: 25 November 2022 doi:10.20944/preprints202211.0478.v1

Figure 13. Photo of two eyebolts installed on some of the WSBs for block-extraction tests.

In the second session of tests, the small and large blocks were applied. The small WSB were the ones used in the first session as they remained in place after the first session without apparent damage. The large WSBs were placed in the left half of the test channel in 40 rows, plus one at the upstream end with cut blocks for top finishing. In total, 100 WSB, 40 half-blocks, and 3 blocks for the upstream row (row 41). In this case, some of the large WSB were prepared for extraction tests with eyebolts, similarly to what was done in the first session in rows #9, #13, #19, #23, #27 and #33.

2.3. Instrumentation

The magnitudes measured during tests were the flow rates in the auxiliary channel, the force needed to extract a single block from the original place at the end of the test and the movements of the WSB.

2.3.1. Flow Rates

Flow rates were continuously recorded with a *Nivus Portable Flowmeter*, model *NFM 750*, with a combined sensor for flow velocity and water depths (**Figure 14**).

Figure 14. Picture of the sensor of the *Nivus Portable Flowmeter* installed in the centre of the auxiliary channel, upstream of the testing chute.

The flowmeter was connected to a *CSM Flow Transducer* (model *CSM-V1D0KN007P*), which uses the operating principle of ultrasonic correlation to determine the speed of water at different water depths, whereby the reflective particles contained in the medium

Preprints (www.preprints.org) | NOT PEER-REVIEWED | Posted: 25 November 2022 doi:10.20944/preprints202211.0478.v1

(minerals, bubbles of air, dirt, etc.) are scanned using ultrasonic pulses transmitted at a certain angle.

2.3.2. Extraction force of a single block from the WSB armoring

The values of the force needed to extract a block installed in the test channel after each session was carried out. The system consisted of a load cell linked to a recording device with a display that allowed to continuously observe the applied effort and that registered the maximum force applied during the entire extraction process. The load cell is the model *Siwarex WL 230 SB-S SA* (*SIEMENS*), for a nominal load of 1 t and precision class C3. It is a shear load cell that is used for both tension and compression loading. The measurement element comes in a hermetic casing and has the output voltage calibrated and proportional to the load. For the recording and visualization of the forces, a *Ditel* brand multifunction digital indicator, the MICRA-M model of the *Kosmos series*, has been used, whose basic functions allow for visualization of the input variable as well as other programmable functions.

2.3.3. Movements of the WSB

The movements of the blocks after each test session were measured by means of the comparison between the 3D digital model of the external surface of the initial and final state. Digital terrain models (DTM) were obtained from photographs with digital cameras processed by *Agisoft PhotoScan Professional v.1.4.3*. The assignation of scale and a reference system to the DTM required a series of known support points (*targets*) that must appear in the different frames. Therefore, 18 targets were generated and adhered to the side walls of the chute (**Figure 15**). Nine of them on the right wall of the chute, numbered from 1 (downstream) to 9 (upstream), and the other nine at the left wall of the chute, numbered from 11 (downstream) to 19 (upstream).

Figure 15. Picture of the targets on the sides of the testing chute.

Two coordinate systems (one relative and one absolute) were used in the process, as shown in **Figure 16**.

Preprints (www.preprints.org) | NOT PEER-REVIEWED | Posted: 25 November 2022 doi:10.20944/preprints202211.0478.v1

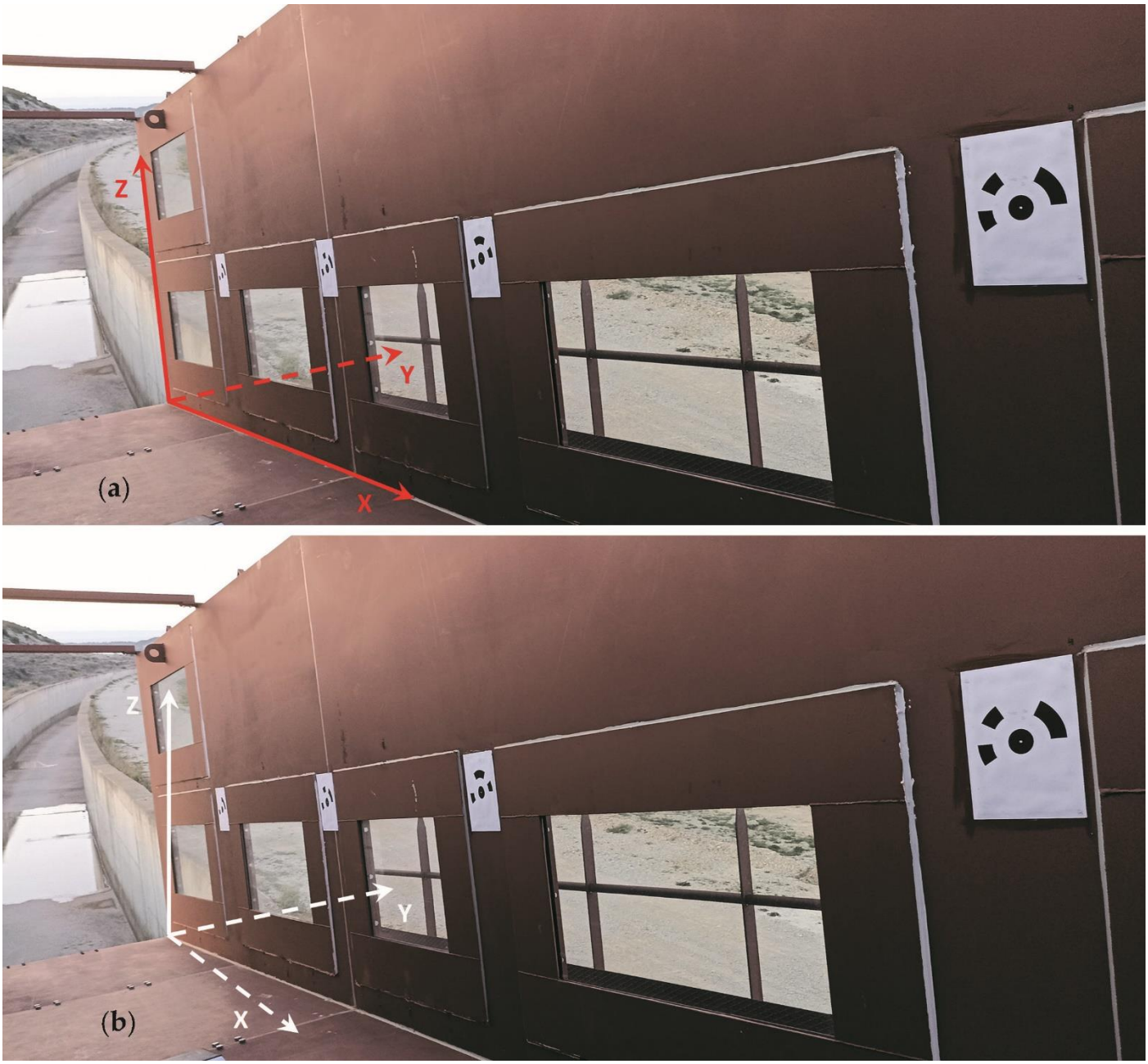

Figure 16. Location of the coordinate systems in the testing chute. (a) Relative (red) and (b) absolute (white).

The coordinates of the markers used, in any of these systems, are reflected in **Table 2**.

Table 2. Relative and absolute coordinates targets.

RELATIVE COORDINATES TARGETS			
TARGET NUM.	**X** mm	**Y** mm	**Z** mm
1	2.102	0.000	1.057
2	3.987	0.000	1.057
3	5.587	0.000	1.057
4	7.591	0.000	1.075
5	9.589	0.000	1.075

ABSOLUTE COORDINATES TARGETS			
TARGET NUM.	**X** mm	**Y** mm	**Z** mm
1	1.407	0.000	1.885
2	3.093	0.000	2.728
3	4.524	0.000	3.444
4	6.309	0.000	4.356
5	8.096	0.000	5.250

Preprints (www.preprints.org) | NOT PEER-REVIEWED | Posted: 25 November 2022 doi:10.20944/preprints202211.0478.v1

6	11.595	0.000	1.064	**6**	9.895	0.000	6.137
7	13.589	0.000	1.064	**7**	11.679	0.000	7.029
8	15.584	0.000	1.051	**8**	13.469	0.000	7.909
9	17.590	0.000	1.072	**9**	15.254	0.000	8.825
11	2.085	-2.008	1.045	**11**	1.398	-2.008	1.867
12	3.963	-2.008	1.050	**12**	3.075	-2.008	2.711
13	5.395	-2.008	1.044	**13**	4.359	-2.008	3.346
14	7.400	-2.008	1.043	**14**	6.152	-2.008	4.242
15	9.408	-2.008	1.043	**15**	7.948	-2.008	5.140
16	11.407	-2.008	1.043	**16**	9.736	-2.008	6.034
17	13.410	-2.008	1.044	**17**	11.527	-2.008	6.931
18	15.410	-2.008	1.044	**18**	13.316	-2.008	7.825
19	17.410	-2.008	1.044	**19**	15.105	-2.008	8.720

3. Results and Discussion

The main results of the two sessions of tests are presented in this chapter. It should be noted that during the first session of tests, both the small and medium sized WSBs were able to withstand the flow rates, with a maximum steady flow of 1.8 m^3s^{-1} and a punctual flow rate peak of 2.0 m^3s^{-1}, without apparent damage. In the second session of tests, the small blocks were pulled downstream for a steady flow rate of 4.7 m^3s^{-1}. The session continued until reaching maximum steady flow rates of 6.8 m^3s^{-1} with maximum peaks of 7.2 m^3s^{-1}, without any damage to the large blocks. However, at the end of the session, during the abrupt decrease in the flow supply from Acequia de Sora (which quickly decreased from more than 7 m^3s^{-1} to less than 1 m^3s^{-1}, in roughly 10 minutes), there was a sudden drag of most of the large blocks and the granular bedding layer. As a result, the session ended and neither the register of WSB movements nor the extraction tests could be performed.

The results are organized in three parts. First, a subchapter describing the overall performance of the tests and the hydraulic loading. The next subchapters are dedicated to describing the movements of the WSB and the extraction tests (only for the first session of tests).

3.1. Hydraulic loading and performance of the WSB armorings.

3.1.1. Test Session 1.

The session began with the filling of both the pressure channel and the supply tower. A constant flow rate of approximately 0.4 m^3s^{-1} was supplied until the elevation of the water surface at the tower achieved the bottom of the upstream section of the testing chute. Subsequently, the flow rate was increased to an average maximum of approximately 1.8 m^3s^{-1}. This discharge was applied for nearly 20 minutes, presenting some peak discharges of 2.0 m^3s^{-1}. After this period, a leak was observed in the joint between the supply tower and the test chute, and the session had to be ended (Video 4 and Video 5 in Supplementary Materials). The total volume of water supplied from Acequia de Sora was 4,000 m^3 of the 58,000 m^3 originally planned for this session.

The inflow hydrograph and the evolution of the water velocities, water depths, and volume of water supply during this session are presented in **Figure 17** with data registered every 5 s.

Preprints (www.preprints.org) | NOT PEER-REVIEWED | Posted: 25 November 2022 doi:10.20944/preprints202211.0478.v1

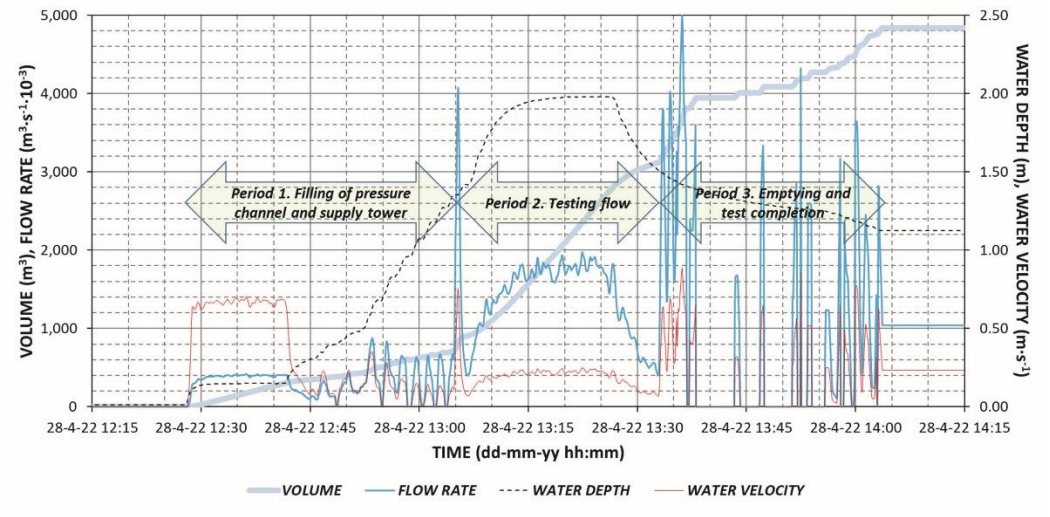

Figure 17. Test Session 1: Inflow hydrograph, water volume, water depth, and flow velocity recorded by the flowmeter at the auxiliary channel.

During Test Session 1, neither the small nor the medium-sized blocks suffered apparent damage with unit flows of 0.9 m^2s^{-1} and peaks up to 1.0 m^2s^{-1}. According to the methodology developed by San Mauro et al. [24] the thickness of the drainage layer should be between 0.60 and 0.95 m. These values were obtained through various calculations in which a sensitivity study was carried out, varying the estimate of seepage based on the investigations carried out by Caballero et al. [23] and San Mauro et al. [25] considering the permeability of the drainage layer. It should be noted that the methodology of San Mauro et al. aims to avoid the existence of uplift pressures in the drainage layer. Therefore, in this case, with a 0.20 m gravel layer, uplift pressures could be developed at the base of the WSB. Such pressures were resisted by the combination of actions such as the weight of the WSB, the positive pressure of the skimming flow that impinges on the upper face of the WSB, the overlapping of the different rows, and the drainage of the seepage flow through the vents of the blocks.

3.1.2. Test Session 2.

In Test Session 2, the pressure channel and supply tower were filled with a flow rate of 0.3 to 0.4 m^3s^{-1} similarly as in Test Session 1. After the filling period, a flow discharge of approximately 0.9 m^3s^{-1} was supplied for 15 minutes. The discharge was increased to 1.7 m^3s^{-1} for another 15 minutes and increased again to 2.5 m^3s^{-1}, which was applied for another 20 minutes, for the total time of approximately 1 hour for these discharges. The next discharge was increased to an average flow rate of 4.7 m^3s^{-1}, with maximum peaks of 5.2 m^3s^{-1} for 20 minutes (Video 6 in Supplementary Materials).

The last discharge was the maximum possible inflow that could be supplied through the control gate. Higher discharges required the operation of the free surface spillway. This operation lasted almost 1 hour, at which time the discharges were significant and the level in the Acequia de Sora increased. At that time, the Acequia intake gate was completely reopened and a discharge of 6.8 m^3s^{-1} was achieved with peaks of 7.2 m^3s^{-1}. This hydraulic loading was continued for more than 10 minutes. That was the maximum discharge that could be achieved with the conditions of the Acequia de Sora at that moment. Therefore, the team decided to end the Test Session by closing the control gate as quickly as possible to save the maximum volume of water. The total volume of water supplied from Acequia de Sora, during approximately 3 hours of the Test Session 2, was almost 30,000 m^3 of the 52,000 m^3 that was planned. The inflow hydrograph and the evolution of the water velocities, water depths, and volume of water supply during this session are presented in **Figure 18** with data registered every 5 s.

Preprints (www.preprints.org) | NOT PEER-REVIEWED | Posted: 25 November 2022 doi:10.20944/preprints202211.0478.v1

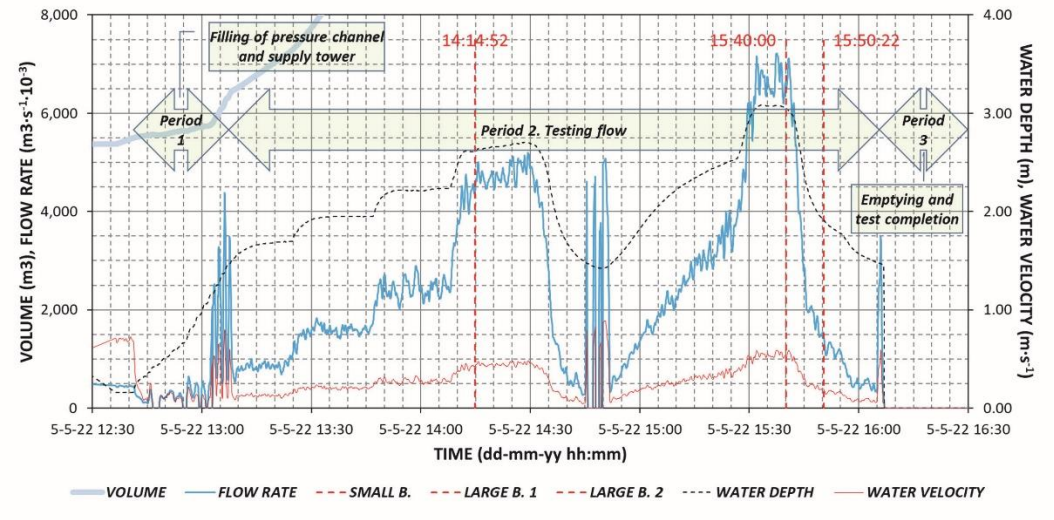

Figure 18. Test Session 2: Inflow hydrograph, water volume, water depth, and flow velocity recorded by the flowmeter at the auxiliary channel.

The performance of the WSB armoring was different for the two sizes of blocks during Test Session 2. Thus, the small WSB could resist unit discharges up to 2.4 m^2s^{-1}. For higher discharges, they were destabilized and completely dragged downstream. The large WSB could resist overflowing discharges of 3.4 m^2s^{-1} with peaks of up to 3.6 m^2s^{-1}. However, it was surprisingly observed that the large WSB were destabilized and were dragged downstream during the closing operations after the session when the overflowing discharge was rapidly decreased, for overflowing discharges significantly lower than the ones that the WSB armoring could resist during the Test Session 2. Thus, the large WSB were completely dragged except for the 4 upper rows.

Similarly to Test Session 1, the minimum thickness of the drainage layer was calculated to avoid uplift pressure and resulted in a range of values between 1.4 and 2.2 m. In this case, the protection was not stable for the small WSB, so the action of the uplift pressures may be one of the possible causes of the protection failure. The large WSB could also be affected by this action during the rapid decrease in overtopping discharge that caused the failure.

3.2. Movements of the surface of the WSB armoring.

The control of movements of the WSB armoring could be performed just in the Test Session 1 due to the dragging of the WSB tested in Test Session 2. Both DTMs were obtained before and after the test session. Each DTM was processed by GIS software to obtain the raster difference between the initial and final DTM and 3 longitudinal profiles for each size of WSB representing the original and the final state, and the difference between the original and the final.

Figure 19 represents the displacements of the points that experience downward movements (from 0 to 5 mm in light green and from 5 to 10 mm in dark green) and upward movements (from 0 to 5 mm in orange and from 5 to 10 mm in red). In general, it can be observed a predominance of the downward vertical displacement of less than 5 mm (light green), with some areas that reach 10 mm (dark green) and even exceed them (in black) reaching up to 20 mm.

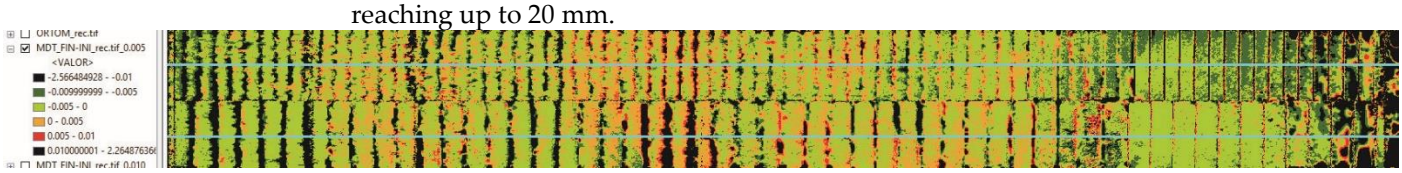

Figure 19. Raster difference between the initial and final DTM. Small blocks in the top half of the coloured area and medium blocks in the lower. The flow direction is from right to left of the figure.

Preprints (www.preprints.org) | NOT PEER-REVIEWED | Posted: 25 November 2022 doi:10.20944/preprints202211.0478.v1

A more detailed representation of the upper rows of the WSB armoring (rows #53 to #81 of the small WSB and #35 to #54 of the medium WSB) is shown in **Figure 20**. In the initial and final zones of the channel, the decrease occurs in complete blocks (mainly green zones) and is especially pronounced in the small blocks of the upper part of the channel (dark green).

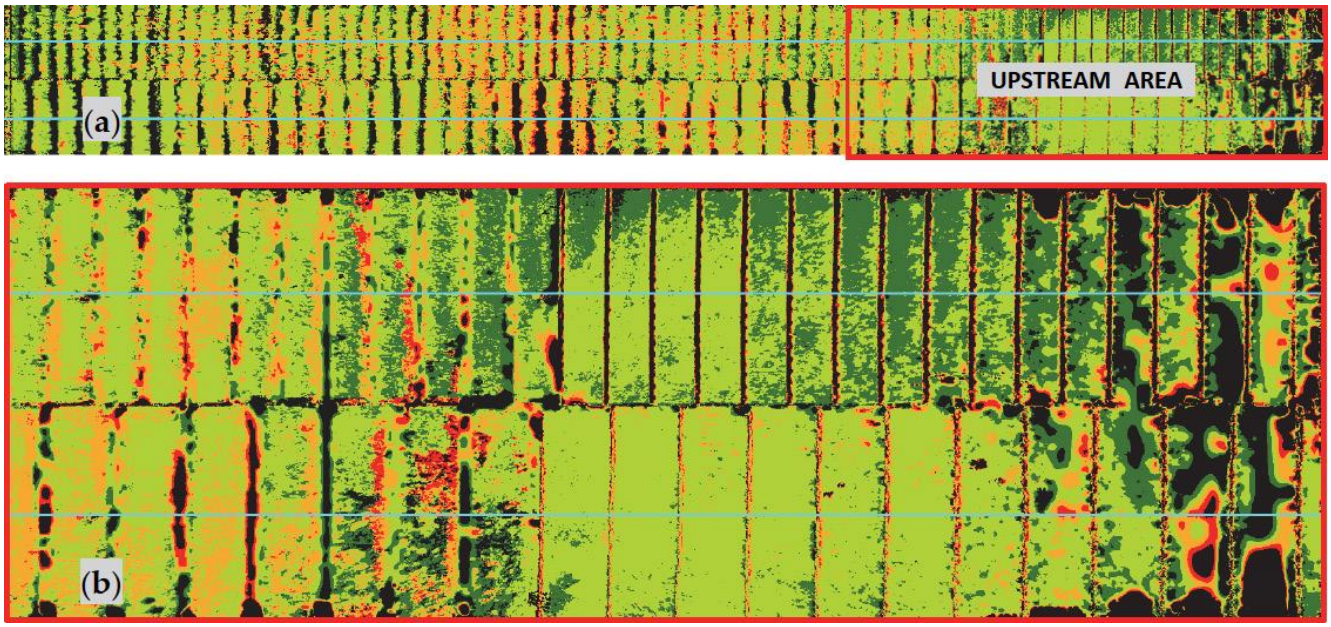

Figure 20. (a) Sketch of the situation of the upper rows in the test chute. (b) Detail of the upstream area of the channel (rows #53 to #81 of the small WSB, in the upper part of the photograph, and rows #35 to #54 of the medium WSB, at the bottom of the figure)

In contrast to the direction of the displacements of the upper rows, upward movements appeared frequently in the lower and central rows, but with values lower than 5 mm (orange colors), and were usually accompanied by areas with downward movements (green colors) within the same row of blocks (**Figure 21**).

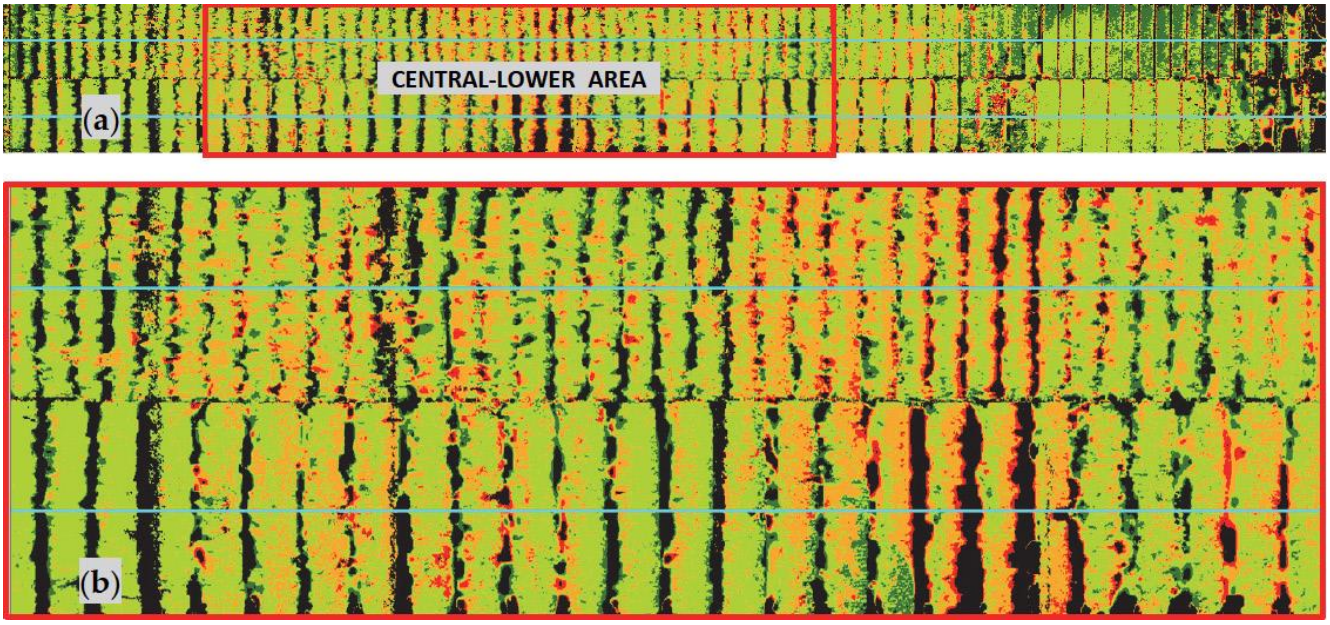

Figure 21. (a) Sketch of the situation of the central-lower rows in the testing chute (b) Detail of the upstream area of the channel (rows #6 to #43 of the small WSB, in the upper part of the photograph, and rows #4 to #29 of the medium WSB, at the bottom of the figure)

Preprints (www.preprints.org) | NOT PEER-REVIEWED | Posted: 25 November 2022 doi:10.20944/preprints202211.0478.v1

The longitudinal profiles of the WSB armoring in the initial and final states, and the differences between both are represented in **Figure 22** (for the small WSB) and **Figure 23** (for the medium WSB). The blue lines in **Figure 19** the position of the axes where the longitudinal cross sections were obtained.

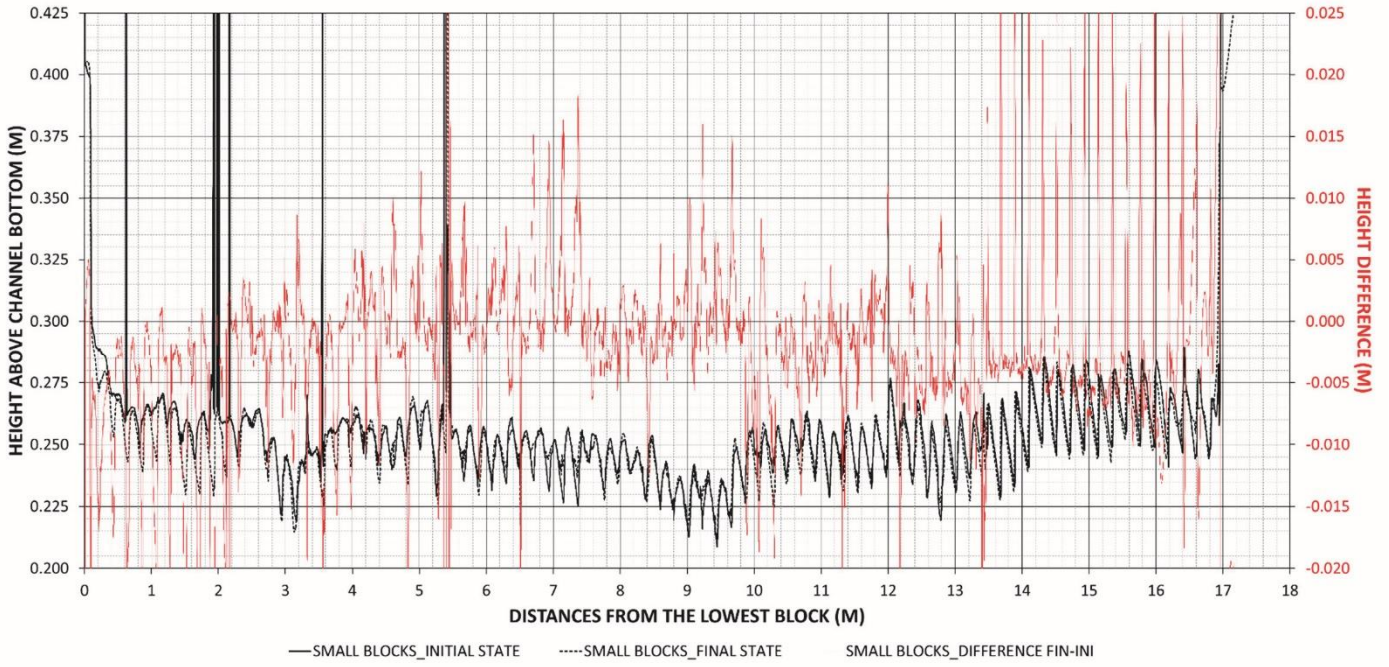

Figure 22. Longitudinal profiles in the small blocks: initial state (continuous black line), final state (continuous dotted line), and difference final vs. initial (red line).

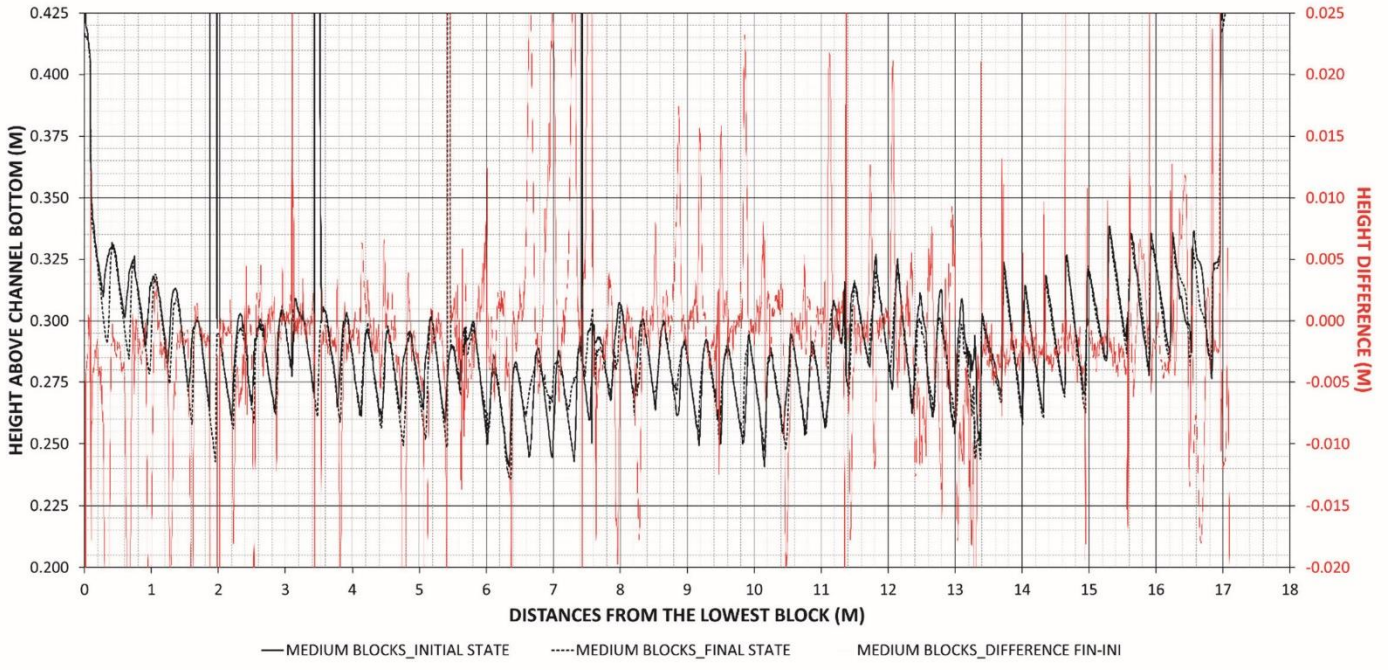

Figure 23. Longitudinal profiles in the medium blocks: initial state (continuous black line), final state (continuous dotted line), and difference final vs. initial (red line).

Figure 24 presents a scheme to help interpret the vertical differences between the original and final DTM presented above. Therefore, **Figure 24** shows a detail of the longitudinal profile of four blocks that have experienced displacements (indicated with grey arrows in **Figure 25**) at the end of the Test Session 1, which justifies the predominance of green

Preprints (www.preprints.org) | NOT PEER-REVIEWED | Posted: 25 November 2022 doi:10.20944/preprints202211.0478.v1

(small negative differences in the upper faces of the WSB) and orange-red black (large positive differences at the downstream edges of the WSB). As can be observed, the armoring direction of the displacement is mainly downstream-downward as could be expected.

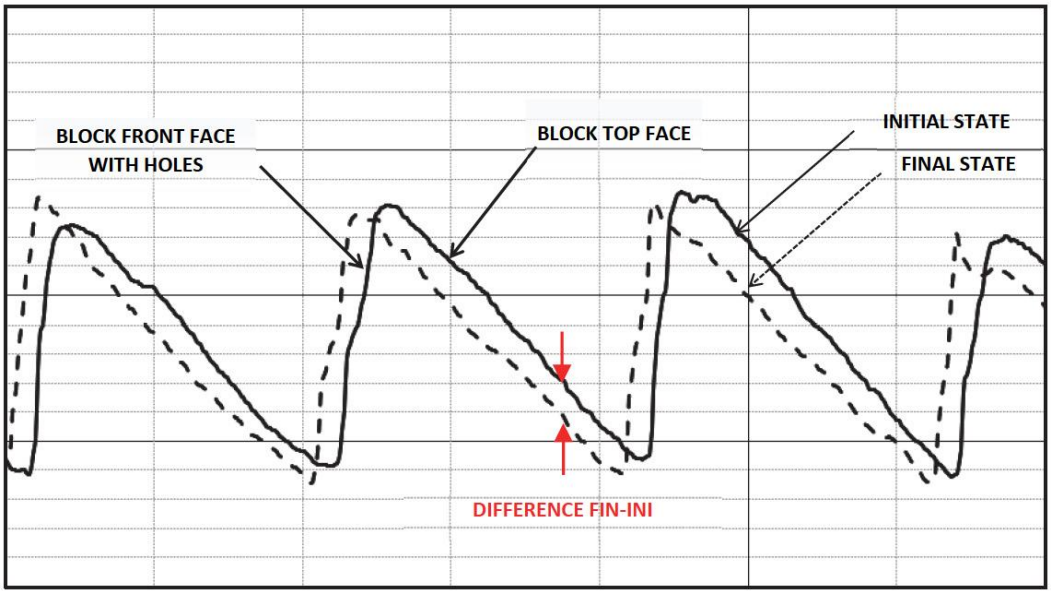

Figure 24. Detail of the longitudinal profile of the WSB armouring. The black dotted lines represent the final state, whilst the continuous black line represents the original state.

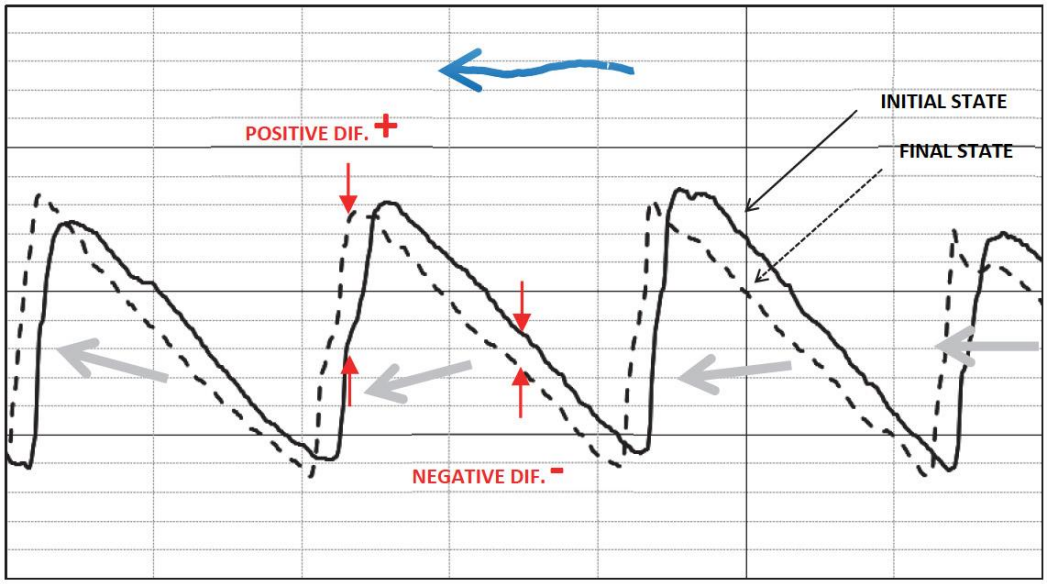

Figure 25. Support scheme for the interpretation of the values obtained.

Thus, the green colors on the upper face of the blocks in **Figure 19** indicate displacement downstream, settlement, or both (so as not to interpret the green colors as settlements of the blocks, since the drop in elevation is due, in general, to its displacement downstream), while the orange-red colors indicate an increase in the external surface of the WSB armoring. A conceptual scheme of the WSB displacements in the longitudinal cross section, considering the vertical and horizontal movements, is presented in Figure 26.

Preprints (www.preprints.org) | NOT PEER-REVIEWED | Posted: 25 November 2022 doi:10.20944/preprints202211.0478.v1

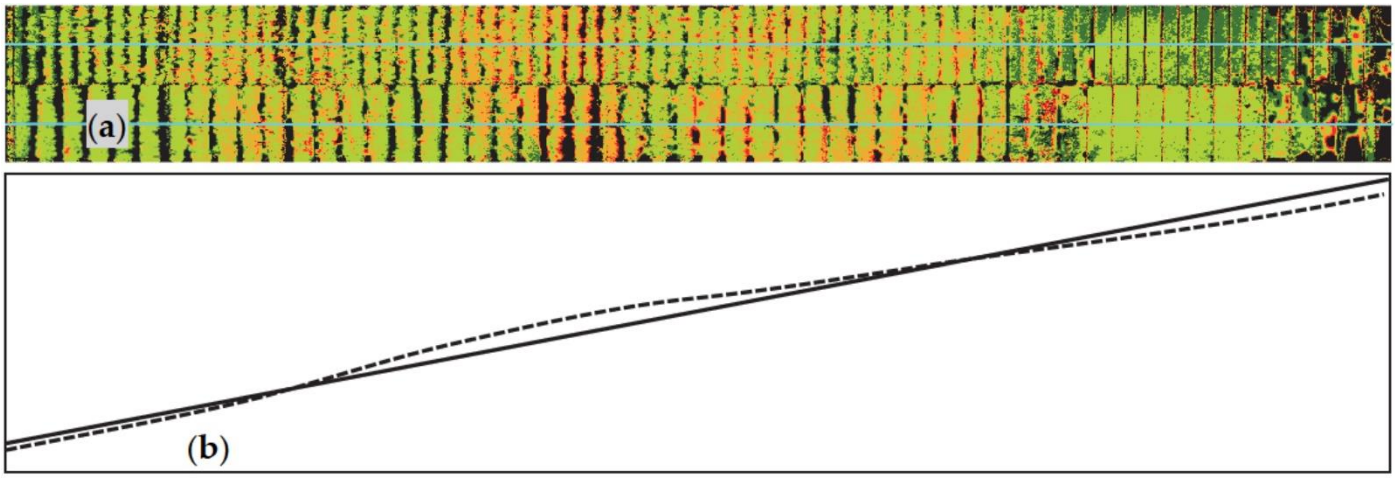

Figure 26. (a) Position of the longitudinal exes in the plan view of the WSB armouring at the testing chute **(b)** Conceptual scheme of the longitudinal profiles of the initial (continuous) and final (discontinuous) states of the WSB armouring in Test Session 1.

The measurement of the movements of the WSB may indicate that there has been a slight displacement of the pieces downstream that increases upstream, which may be due to a readjustment of the pieces locally, reducing the gaps between consecutive rows. This displacement is especially noticeable in the upper and lower rows. The WSB of the upper rows show a slight settlement whilst the ones in the central zone, and especially the central-lower one, present a slight rise and tilt. Some of the possible causes that could lead to the movements registered in the WSB armoring can be the sliding of the granular layer (or the WSB over it) towards downstream, the buckling of the surface of the WSB armoring, the dynamic hydraulic pressures, vibrations in the chute, the uplift pressures under the WSB, or the development of stagnation pressures in the support of the WSB armoring at the downstream end of the testing chute, among others.

3.3. Measurement of the forces needed to extract the WSB from the armoring system

Measurements could be done just in the Test Session 1 for the medium WSB, once the testing chute was empty of water. As mentioned in Section 3, the extracted WSB was the central block of rows #10 (Video 7 and Video 8 in Supplementary Materials), #18, #24, #30, #36 and #42. The results of the extraction tests are shown in **Table 3**.

Table 3. Measurements of forces needed to extract the medium WSB after Test Session 1.

Extraction Num.	**Row** (from downstream)	**X*** m	**Z*** m	**Force** N
-	42	13.10	6.55	-
1	36	11.23	5.62	2,768.4
-	30	9.36	4.68	-
2	24	7.49	3.74	3,946.6
4	18	5.62	2.81	918.2
3	10	3.12	1.56	3,089.2
Total length (m)	16.54			
Total drop (m)	8.27			

* Distance X from the lowest block and Height Z above channel bottom

As can be observed in **Table 3**, the average force needed to extract the medium WSB (with a weight of 147 N each block) in the 4 trials is 2680 N, which is more than 18 times

Preprints (www.preprints.org) | NOT PEER-REVIEWED | Posted: 25 November 2022 doi:10.20944/preprints202211.0478.v1

the WSB weight. Peak values of 918 N (roughly six times the weight of the block) and 3945 N (27 times higher). According to the results of **Table 3** it is not possible to establish a relationship between the extraction force and the WSB position of the row along the testing chute. The extraction forces are so high in comparison with the WSB weight due to the overlapping of the rows and the staggered placement, which makes it necessary to mobilize several blocks around the WSB which is pulled out from the original place.

3.4. Disscusion on the Performance of the WSB armoring

During the testing time (i.e., operation under steady flow steps, gradually increased between them) of the two sessions of tests, the armoring composed of small WSB failed for a unit discharge of 2.4 m^2s^{-1}. Medium and large WSBs were stable for maximum unit discharges of 1 and 3.6 m^2s^{-1}, respectively, which was the maximum available at the facility in the days when tests were performed. It should be noted that armoring with medium WSB could not be tested for unit discharges greater than 1 m^2s^{-1}. Nevertheless, the armoring with the large WSB failed during the closing operation to empty the test chute. The failure occurred several minutes after the end of the test session, during a rapid drop in flow rate and for a unit discharge lower than 3.6 m^2s^{-1} (i.e., the maximum unit discharge used in the testing time). Some of the possible causes of such failure are discussed next, but further investigations should be carried out to confirm or refute them.

Excessive uplift pressures could be one of the causes of failure. In addition, during the emptying time, there was a quick reduction in the depth of the water and the positive pressure at the top of the WSB. Additionally, the reduction in flow velocity could lead to a lower stabilizing force caused by hydraulic suction under the WSB.

Another cause could be an insufficient drainage capacity of the supporting drainage layer for a quick reduction in skimming flow. Furthermore, the perforated metal plate, where the downstream row of the WSB was supported (**Figure 27**), could lead to a lack of drainage that resulted in an increase in uplift pressure under the lower rows of WSB. Such a metal plate at the downstream end formed was an obstacle for the skimming flow due to the offset between the pseudo bottom of the stepped WSB armoring and the upper part of the metallic plate. This configuration could lead to hydraulic jacking due to the development of the stagnation pressure due to the transformation of the kinetic energy of the flow into pressure energy, causing dynamic pressures that are transmitted to the base, destabilizing the downstream rows of WSB.

Figure 27. Detail of the perforated metal plate, where the downstream row of the WSB was supported

4. Conclusions.

The experimental research carried out to test the new model of WSB (ACUÑA) involved the construction of a large experimental facility (HEFLR) capable to carry out tests

 doi:10.20944/preprints202211.0478.v1

on a quasi-prototype size with maximum discharges of up to 7 m^3s^{-1} and maximum unit flow rates of up to 14 m^2s^{-1} with the minimum width of 0.5 m in the testing chute. HEFLR aims to be an experimental installation for the future evaluation of the performance of systems or technologies for the overflowing protection of dams and levees in quasi prototype conditions, with high hydraulic loadings.

WSB armoring tests with ACUÑA model were performed for three different sizes (small, medium and large, of 5, 15 and 35 kg, respectively). The armoring with the small size units failed for a unit discharge of 2.4 m^2s^{-1}. The medium size was tested for a maximum unit discharge of 1.0 m^2s^{-1} and no damage was observed. Finally, the large WSB could resist unit discharges of 3.4 m^2s^{-1}, with peaks of up to 3.6 m^2s^{-1} without damage during the testing time. However, a failure of the armoring with the large WSB suddenly occurred during the emptiness operation, at the end of the test for lower unit discharges than those applied during the testing time.

In the test session in which the WSB armoring remained in place at the chute after the testing time and emptying operation, the displacements of the blocks were recorded. Such movements were generalized but not relevant, slightly larger in small WSB than in medium. In general, the displacements showed settlement (from 0 to 10 mm) and downstream sliding (from 0 to 5 mm) with a minor elevation (0 to 5 mm) of the WSB in the rows located in the central area of the testing chute.

A total of 4 extraction tests were performed after the end of the first session of tests on medium-sized blocks. The average force needed to pull out the blocks weighing 147 N (15 kp) was 2680 N (273.25 kp) which is more than eighteen times their weight, due to the overlapping of the rows and the staggered placement, which makes it necessary to mobilize several blocks around the WSB which is pulled out from the original place. No relationship could be inferred between the required extraction force and the WSB position of the row in the armoring.

Finally, the need for further research to complement the results presented in this article is evident. In the new research, the installation should be carried out to avoid the formation of stagnation pressures at the downstream end, recording the evolution of the pressures at the base of the blocks to determine the evolution of the uplift pressures. In addition, a study should be carried out on the stability conditions of the granular support layer, testing possible improvements such as the use of geocells, among others.

Supplementary Materials: The following are available online at www.mdpi.com/xxx/: Experimental_set_up and test sessions (8 videos): VIDEO_01_Intake_work_GATE_closed; VIDEO_02_Intake_work_GATE_open; VIDEO_03_Chute_lowered_by_crane; VIDEO_04_Test 01_from_downstream; VIDEO_05_Test 01 from_methacrylate_windows; VIDEO_06_Qmax_Test02; VIDEO_07_Extraction_test_01_row10 (1); VIDEO_08_Extraction_test_01_row10 (2)

Authors Contributions: Conceptualization, F.J.C., R.M., M.Á.T. and J.P.; methodology, F.J.C., R.M., M.Á.T., and J.P.; formal analysis, F.J.C., R.M., M.Á.T., and J.P.; investigation, F.J.C. and J.P.; data curation, J.P.; visualization, J.P..; writing—original draft preparation, F.J.C. and J.P.; writing—review and editing, R.M. and M.Á.T.; supervision, R.M. and M.Á.T. All authors have read and agreed to the published version of the manuscript.

Funding: This research was funded by the Spanish Ministry of Science and Innovation (Ministerio de Ciencia e Innovación, MICINN) through the PABLO project (grant number RTC-2017-6196-5).

Data Availability Statement: Data are available on request.

Acknowledgments: The authors would like to acknowledge the collaboration of Luis Ruano† from PREHORQUISA, without whose involvement these projects would not have been possible, and the Red de Aulas CIMNE. Also to the Bardenas Channel Irrigation Association as a user; ACUAES (Aguas de las cuencas de España) as an operator; and Ebro River Basin Authority as an owner, by the transfer of preexisting infrastructures for use with research purposes. And the company ACIS2in, which has collaborated with the R+d Consortium (formed by the company PREHORQUISA, the Universidad Politécnica de Madrid, UPM, and the International Center for Numerical Methods in Engineering, CIMNE) in the execution of the tests during the year 2022.

Finally, the authors would also like to acknowledge María Monterde from PREHORQUISA; Ricardo Monteiro-Alves from the Dam Safety Research Group (SERPA) of UPM; Fernando Salazar and Javier San Mauro from CIMNE; and Iván Gabriel from ACIS2in.

Conflicts of Interest: The authors declare that they have no conflict of interest.

References

1. ICOLD Bulletin No. 99. Dam failures - statistical analysis. International Commission on Large Dams (ICOLD), 1995.
2. FEMA. Technical manual: Overtopping protection for dams U.S. Department of Homeland Security. 2014
3. Hewlett, H., Baker, R. May, R., and Pravdivets, Y.P. Design of stepped-block spillways. London, UK: Construction Industry Research and Information Association. 1997
4. Grinchuk, A.S. and Pravdivets, Y. P. and Shekhtman. Test of earth slope revetments permitting the flow of water at large specific discharges. Translated from *GidrotekhnicheskoeStroitel stvo,* April 1977 nº4, pp. 22-26.
5. Pravdivets, Y.P. and Slissky, S. M. Passing floodwaters over embankment dams. *International Water Power and DamConstruction* 1981, 33(7), 30-32.
6. Baker, R. and Gardiner, K. Construction and performance of a wedge block spillway at Brushes-Clough reservoir. Proceedings of the 8th Conference of the British Dam Society on Reservoir Safety and the Environment, 1994, 214-223.
7. Baker, R., Pravdivets, Y., and Hewlett, H. Design considerations for the use of wedge-shaped precast concrete blocks for dam spillways. Proceedings of the Institution of Civil Engineers-Water and Maritime Engineering 1994, 106(4), 317-323.
8. Baker, R. and Gardiner, K.D. Building blocks. *International Water Power and Dam Construction* 1995, vol. 47, no. 11, pp. 2.
9. Bramley, M. and May, R. and Baker, R. Performance of wedge-shaped blocks in high-velocity flow. CIRIA Research Project 407. Stage 1 Report- July 1989.
10. Bramley, M. and May, R. and Baker, R. Performance of wedge-shaped blocks in high-velocity flow. CIRIA Research Project 407. Stage 2 Report- July 1991.
11. Cloppper, P.E. Hydraulic stability of articulated concrete block revetment systems during overtopping flow. 1989
12. Slovensky Jr., G.G. Near-prototype testing of wedge-block overtopping protection. M.S. thesis, Colorado State University, Colorado, United States. 1993
13. Gaston, M. L. Air entrainment and energy dissipation on a stepped block spillway. M.S. thesis, Colorado State University, Fort Collins, CO. 1995.
14. Frizell, K. H., Protecting embankment dams with concrete stepped overlays. *Hydro Review* 1997 September 16, 36-45.
15. Frizell, K.H. Armorwedge™ analysis report: block size scaling and bedding information. 2007 (Confidencial).
16. Thornton, CI, Robeson, M.D., Varyu, D.R. Armorwedge™ data report 2006 testing for armortec erosion control solutions, inc. Unpublished manuscript (confidential).
17. Relvas, A.T. and Pinheiro, A.N. Closure of "Inception Point and Air Concentration in Flows on Stepped Chutes Lined with Wedge-Shaped Concrete Blocks". *Journal of Hydraulic Engineering* 2010, Vol.136, issue 1, 86-88
18. Relvas, A.T. Descarregadores de Cheias de Blocos de Betão Prefabricados em Forma de Cunha sobre Barragens de Aterro (in Portuguese). Ph.D. Thesis, Universidade Tecnica de Lisboa, Instituto Superior Técnico. 2008.
19. Relvas, A.T. and Pinheiro, A.N. Inception point and Air Concentration in flows on Stepped Chutes Lined with wedge-shaped concrete blocks. *Journal of Hydraulic Engineering* 2008, Vol.134, issue 8, 1042-1051
20. Relvas, A.T. and Pinheiro, A.N. Stepped chutes lined with wedge-shaped concrete blocks: hydrodynamic pressures on blocks and stability analysis. *Canadian Journal of Civil Engineering* 2011, 38, 338-349
21. Relvas, A.T. and Pinheiro, A.N. Velocity Distribution and Energy Dissipation along Stepped Chutes Lined with Wedge-Shaped Concrete Blocks. *Journal of Hydraulic Engineering*, 2011, Vol. 137, No. 4, April, 423–431
22. Morán, R. Wedge-shaped blocks: A Historical Review. 2nd International Seminar on Dam Protections against Overtopping. Protections 2016. Colorado State University (CSU). 2016 https://mountainscholar.org/handle/10217/179790
23. Caballero, F.J.; Toledo, M.Á.; Moran, R.; San Mauro, J. Hydrodynamic Performance and Design Evolution of Wedge-Shaped Blocks for Dam Protection against Overtopping. *Water* 2021, *13*, 1665. https://doi.org/10.3390/w13121665
24. J. San Mauro, M. Toledo, F. Salazar and F. F.J.Caballero, A methodology for the design of dam spillways with wedge-shaped blocks based on numerical modeling, *Revista Internacional de Métodos Numéricos para Cálculo y Diseo en Ingeniería (RIMNI)* 2018. (Online first). URL https://www.scipedia.com/public/San_Mauro_et_al_2018a
25. San Mauro, J.; Larese, A.; Salazar, F.; Irazábal, J.; Morán, R.; Toledo, M. Á. Hydraulic and stability analysis of the supporting layer of wedge-shaped blocks. 2nd International Seminar on Dam Protections against Overtopping and Accidental Leakage. Protections 2016. Colorado State University (CSU). 2017 https://mountainscholar.org/handle/10217/17978